ISSN 0280–5316
ISRN LUTFD2/TFRT--5654--SE

Feedback control of plasma position in the EXTRAP-T2 fusion experiment

Filip Lindau

Department of Automatic Control
Lund Institute of Technology
November 2000

Department of Automatic Control
Lund Institute of Technology
Box 118
SE-221 00 Lund Sweden

Document name
MASTER THESIS

Date of issue
November 2000

Document Number
ISRN LUTFD2/TFRT--5654--SE

Author(s)
Filip Lindau

Supervisor
P. Brunsell (KTH)
P. Hagander (LTH)

Sponsoring organisation

Title and subtitle
Feedback control of plasma position in the EXTRAP-T2 fusion experiment

Abstract

Automatic control of the plasma radial position, extracted from magnetic measurements, in EXTRAP-T2 is simulated. A simple model of plasma, surrounding copper shell and vertical field coils have been used. Design is concentrated on the PD type of controller with parameters studied in relation to power supply performance, i.e. switching frequency and maximum output voltage. Effects of saturation, noise and feed forward are examined. The controller is also tested with real sensor data from earlier shots.

Key words
control, PD controller, plasma radial position, fusion, RFP

Classification system and/or index terms (if any)

Supplementary bibliographical information

ISSN and key title
0280–5316

ISBN

Language
English

Number of pages
1–40

Recipient's notes

Security classification

Contents

List of Figures

1 Introduction

1.1 Background

A majority of fusion experiments are based on the TOKAMAK (acronym created from the Russian words, "TOroidalnaya KAmera ee MAgnitnaya Katushka," or "Toroidal Chamber and Magnetic Coil") configuration. It is characterized by a large externally applied toroidal magnetic field, and a smaller poloidal field generated by plasma current, to provide confinement. The toroidal field coils require huge amounts of power or must be made of superconducting material.

The experiment in Alfvénlaboratoriet, EXTRAP-T2, is of the reversed field pinch (RFP) type. Here the plasma itself generates most of the magnetic field, with toroidal and poloidal components of comparable amplitudes. Among the advantages of an RFP reactor compared to a TOKAMAK are higher energy density and ability to reach ignition without auxiliary heating. This would lead to a more compact and economical reactor.

1.2 Problem description

Normally RFP experiments rely on a perfectly conducting shell that stabilizes plasma instabilities through induction. In a reactor this approximation would not be valid due to long pulse times during which the magnetic field would have time to penetrate the shell. In EXTRAP the problem with a resistive shell is studied; the shell penetration time is 5 ms compared to pulse times around 20 ms. The stabilizing effect of the shell is then reduced and active feedback is required.

While the copper shell can take care of variations in plasma position on time scales smaller than the penetration time, the controller has to handle slower fluctuations. Using a preprogrammed vertical magnetic field, the plasma can be centered under constant conditions. Looking at earlier shots, it can be seen clearly that the plasma drifts radially during the shot. Eventually it hits the wall and the pulse is terminated. With a feedback system keeping the plasma centered the pulse length could hopefully be increased and the experimental results more reproducible. The design goals for the controller have been a settling time $\tau \lesssim 1$ ms and a phase margin $\varphi \geq 30°$.

2 Model

2.1 Components

The following parts of the experiment are modelled:

- Plasma
- Copper shell
- Vertical field (control) coils
- Power supply

Only a simple representation will be considered here. Following the lines of the paper from the CLEO experiment [3], plasma, copper shell and vertical field

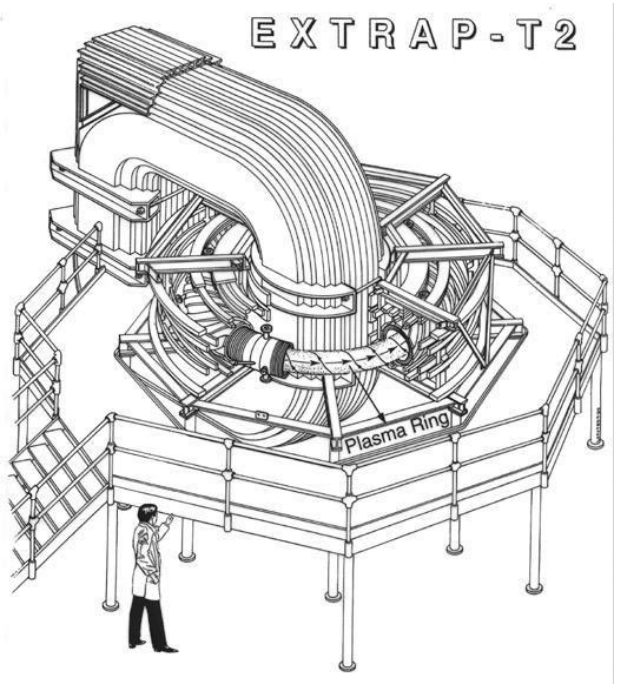

Figure 1: Overview of the EXTRAP-T2 experiment

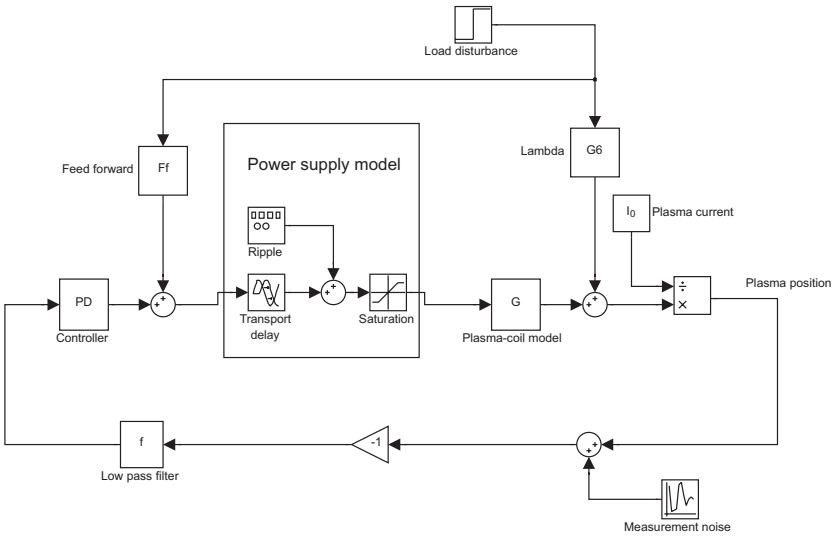

Figure 2: Block diagram of the control loop

coils are modelled with an equation of motion for the plasma and two circuit equations for coil and shell. A switching power supply is assumed, even though the specifics are not yet determined. It is modelled as a limiter and a time delay. See figure 2 for an overview.

Although the sensors measure induced voltage and the signals have to be integrated to get magnetic flux density their dynamics are neglected.

2.2 Equations

For a detailed derivation of the plasma equation of motion, see [3]. The result (valid for small displacements x) is

$$\frac{d^2x}{dt^2} = -\Omega_F^2 x \tag{1}$$

with

$$\Omega_F^2 = \frac{\mu_0 I_0^2}{2R_0 M}\left[(1+m)\Gamma_0 - \frac{1}{2}\right] \tag{2}$$

Stability requires Ω_F^2 to be positive which leads to a minimum value for the vertical field gradient index $m > -1 + \frac{1}{2\Gamma_0}$

A few rather suspicious assumptions had to be made. In particular one concerning toroidal flux conservation leading to a relation between plasma minor radius and position:

$$\left(\frac{a}{a_0}\right)^2 = \frac{R}{R_0} \tag{3}$$

In T2 the plasma fills up the vacuum vessel and is bounded by the molybdenum limiters along the inner wall. It would then perhaps be more appropriate to use (see HBTX1A [5])

$$a = a_0 - |x| \tag{4}$$

and that changes the $\frac{1}{2}$ in Ω_F^2 and with it the stability requirement for m. However, the assumptions from CLEO has been used here.

Forces from currents in the copper shell and the control coils also act on the plasma and have to be accounted for.

$$M\left(\frac{d^2x}{dt^2} + \Omega_F^2 x\right) = \frac{d}{dx}\left(L_{13}I_1I_3 + L_{12}I_1I_2\right) = \frac{2}{\pi b}\left(L_{22}I_1I_2 + L_{23}I_1I_3\right) \tag{5}$$

Here index 1 stands for plasma circuit, index 2 for the conducting shell eddy currents and index 3 for the VF coil circuit. The last step comes from expressions for L_{12} and L_{13}, they are both of the form $L_{1k} = \frac{2}{\pi b} x L_{2k}$ (see B.3 and B.4). Index k can stand for both 2 and 3. As the mass M of the plasma particles is very small the inertial term $M\frac{\partial^2 x}{\partial t^2}$ can be neglected. To test this a computation with the mass included was made. It was found that the system has a resonance peak at around $\omega = 5{\cdot}10^6$ rad/s, well outside the range of interesting frequencies.

Moving on to the circuit equations we have

$$0 = I_2R_2 + \frac{d}{dt}(I_1L_{12}) + L_{22}\frac{dI_2}{dt} + L_{23}\frac{dI_3}{dt} \tag{6}$$

$$V = I_3R_3 + \frac{d}{dt}(I_1L_{13}) + L_{23}\frac{dI_2}{dt} + L_{33}\frac{dI_3}{dt} \tag{7}$$

for the shell and control coils respectively (The inductances L_{22}, L_{23} and L_{33} are constant). The time derivatives of the inductances can be rewritten:

$$\frac{d}{dt}(I_1 L_{1k}) = \frac{dL_{1k}}{dx}\frac{d}{dt}(xI_1) = \frac{2L_{2k}}{\pi b}\frac{d}{dt}(xI_1) \tag{8}$$

The first step comes from

$$\frac{d(I_1 L_{1k})}{dxI_1} = \frac{d(xI_1\frac{dL_{1k}}{dx})}{dxI_1} = \frac{dL_{1k}}{dx} \tag{9}$$

It turns out that xI_1 is a natural control variable. The circuit equations contain it and the sensors measure it (as xI_1 is proportional the flux enclosed by the plasma). To simplify things xI_1 will sometimes be called Ξ. After multiplication by I_1 and linearization, equation 5 becomes (the currents I_2 and I_3 are much smaller than I_1)

$$M\Omega_F^2\Xi = \frac{2I_0^2}{\pi b}(L_{22}I_2 + L_{23}I_3) \tag{10}$$

All three equations assembled in matrix form:

$$\begin{bmatrix} \frac{2}{\pi b}L_{22} & L_{22} & L_{23} \\ \frac{2}{\pi b}L_{23} & L_{23} & L_{33} \\ 0 & 0 & 0 \end{bmatrix}\begin{bmatrix} \dot{\Xi} \\ \dot{I}_2 \\ \dot{I}_3 \end{bmatrix} + \begin{bmatrix} 0 & R_2 & 0 \\ 0 & 0 & R_3 \\ -M\Omega_F^2 & \frac{2I_0^2}{\pi b}L_{22} & \frac{2I_0^2}{\pi b}L_{23} \end{bmatrix}\begin{bmatrix} \Xi \\ I_2 \\ I_3 \end{bmatrix} = \begin{bmatrix} 0 \\ 1 \\ 0 \end{bmatrix} V \tag{11}$$

or

$$\mathtt{E}\dot{\mathtt{x}} - \mathtt{A}\mathtt{x} = \mathtt{B}\,\hat{V} \tag{12}$$

where $\mathtt{x} = [\Xi\ I_2\ I_3]^T$. The set of equations is Laplace-transformed

$$(s\mathtt{E} - \mathtt{A})\hat{\mathtt{x}} = \mathtt{B}\hat{\mathtt{u}} \tag{13}$$

and the displacement $\hat{\Xi}$ solved for with e.g. Maple. The resulting transfer function from $\hat{V}$ to $\hat{\Xi}$ is of the form

$$G(s) = \frac{K}{(1+\frac{s}{\omega_1})(1+\frac{s}{\omega_2})} \tag{14}$$

The numerical values are: $\omega_1 = 161.5$ rad/s and $\omega_2 = 3.1$ rad/s.

2.3 Power supply

As mentioned above the power supply is modelled as a time delay. Its transfer function becomes

$$W(s) = e^{-Ts} \tag{15}$$

with a delay T corresponding to half the switching time $\frac{1}{f_{PS}}$ of the power supply. A first order Pade approximation of this transfer function is

$$W_P = \frac{\frac{2}{T} - s}{\frac{2}{T} + s} \tag{16}$$

It is valid for small ω but quite adequate for the range of interesting control frequencies ($\omega \lesssim 10^4$). Another aspect that is modelled is output voltage saturation, causing non-linear effects. One suggested type of power supply would use IGBT (Insulated Gate Bipolar Transistor) as switching components. They typically have a rating of around 800 V.

Finally, ripple with the switching frequency and unknown amplitude will be present.

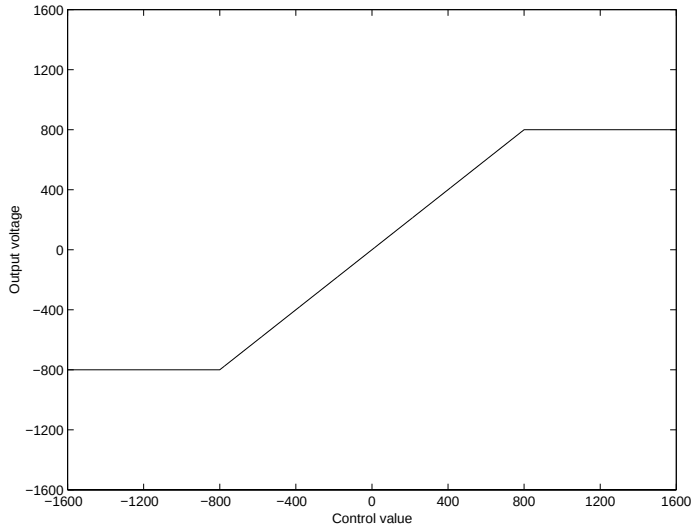

Figure 3: Output voltage saturation

2.4 Disturbances

Various disturbances can be introduced into the equations, e.g. variations in plasma parameters $\delta\Lambda$ or vertical magnetic field δB_z.

In the approximate model used here, $\delta\Lambda$ will not induce any currents in the shell and VF coil directly, but affects the plasma equation of motion. An expression of the total radial force acting on the plasma is (see CLEO [3])

$$f = 2\pi R I_1 (B_{ze} - B_z) \tag{17}$$

with the equilibrium field

$$B_{ze} = \frac{\mu_0 I_1 \Gamma}{4\pi R} \tag{18}$$

and

$$\Gamma = \ln(\frac{8R}{a}) - \frac{1}{2} + \Lambda \tag{19}$$

Differentiation with respect to Λ around the equilibrium position gives

$$\delta f = 2\pi R_0 I_0 \frac{\mu_0 I_0}{4\pi R_0}\,\delta\Lambda = \frac{\mu_0 I_0^2}{2}\,\delta\Lambda \tag{20}$$

Adding this, and remembering to multiply by I_0, the matrix equation becomes

$$(s\mathtt{E} - \mathtt{A})\hat{\mathtt{x}} = \mathtt{B}\,\hat{V} + \begin{bmatrix} 0 \\ 0 \\ -\frac{\mu_0 I_0^3}{2} \end{bmatrix} \hat{\delta\Lambda} \tag{21}$$

The resulting transfer function from $\hat{\delta\Lambda}$ to $\hat{\Xi}$ is of the form

$$G_\Lambda(s) = -K_\Lambda \frac{(1 + \frac{s}{\omega_1^\Lambda})(1 + \frac{s}{\omega_2^\Lambda})}{(1 + \frac{s}{\omega_1})(1 + \frac{s}{\omega_2})} \tag{22}$$

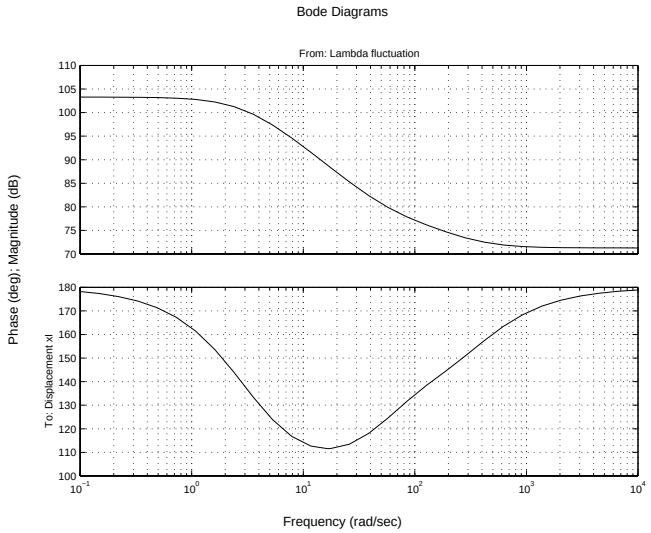

Figure 4: Bode diagram of G_Λ

Numerical values for the zeros are: $\omega_1^\Lambda = 290.9$ rad/s and $\omega_2^\Lambda = 68.7$ rad/s. The effect of the resistive shell can be seen here as a damping of high frequencies (figure 4).

A disturbance in the vertical field δB_z acts differently because it also induces currents in the shell (and coils). This adds terms proportional to $\frac{d\delta B_z}{dt}$ to the circuit equations. The coupling coefficients, here called D_{2B} and D_{3B}, can be calculated in the same way as inductances. Differentiation of the force expression is simply $\delta f = 2\pi R_0 I_0 \, \delta B_z$. The sign of δB_z is chosen so that positive δB_z compresses the plasma.

$$(s\mathtt{E} - \mathtt{A})\hat{\mathtt{x}} = \mathtt{B}\,\hat{V} + \begin{bmatrix} sD_{2B} \\ sD_{3B} \\ -2\pi R_0 I_0^2 \end{bmatrix} \delta\hat{B}_z \tag{23}$$

A calculation of the transfer function from $\delta\hat{B}_z$ to $\hat{\Xi}$ yields

$$G_B(s) = -K_B \frac{1 + \frac{s}{\omega_1^B}}{(1 + \frac{s}{\omega_1})(1 + \frac{s}{\omega_2})} \tag{24}$$

Where $\omega_1^B = 127.2$ rad/s. In this case the shell acts as a first order low-pass filter (see figure 5).

3 Sensors

3.1 Setup

Signals from three different sensors have to be combined to get the plasma position:

- Differential flux loops or saddle coil (average vertical magnetic field, B_{vf})

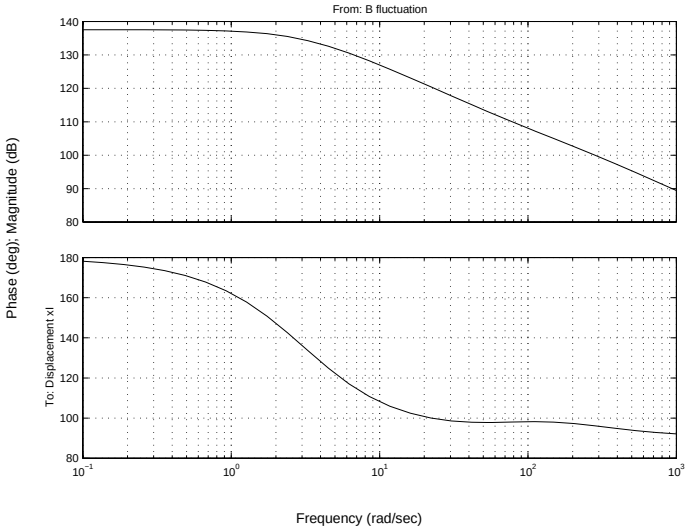

Figure 5: Bode diagram of G_B

- Cosine coil (asymmetric part of the poloidal magnetic field, B_{cos})
- Rogowski coil (plasma current, I_1)

See [4] for a detailed description of the procedure. The effect of the liner current is neglected here.

In a more simple version only the vertical field sensor would be used. The controller would then regulate so as to achieve zero vertical flux. This has been tried in the CLEO experiment [3] with limited success. The problem with this configuration is that it is not possible to distinguish between actual plasma movement and disturbances that change vertical flux (such as δB_z). The system will also be of higher order (because of components $\sim I_2$ in the expression for B_{vf}) and harder to control.

Figure 6 shows how the different sensors are positioned. The cosine coil is comprised of the two B_p solenoids making detection of first harmonic fields possible ($\sim \cos\theta$). Two or more solenoids may be added at different angles to suppress higher order fields ($\cos 2\theta$, $\cos 3\theta$ etc.).

3.2 Equations

Starting from an expression for the flux function $\Psi(r,\theta)$, magnetic field components are obtained through $\mathbf{B} = -\nabla\Psi$. B_{cos} and B_{vf} are then identified from the expressions. The unknowns are xI_1 and Λ (or B_z^{ext}, depending on the choice of flux function). The resulting equations are (using B_z^{ext}):

$$\begin{bmatrix} -\frac{\mu_0}{2\pi r_c^2} & k_{zc} \\ \frac{\mu_0}{2\pi r_{vf}^2} & k_{zvf} \end{bmatrix} \begin{bmatrix} xI_1 \\ B_z^{ext} \end{bmatrix} = \begin{bmatrix} B_{cos} \\ B_{vf} \end{bmatrix} - \begin{bmatrix} k_{pc} \\ k_{pvf} \end{bmatrix} I_1 \tag{25}$$

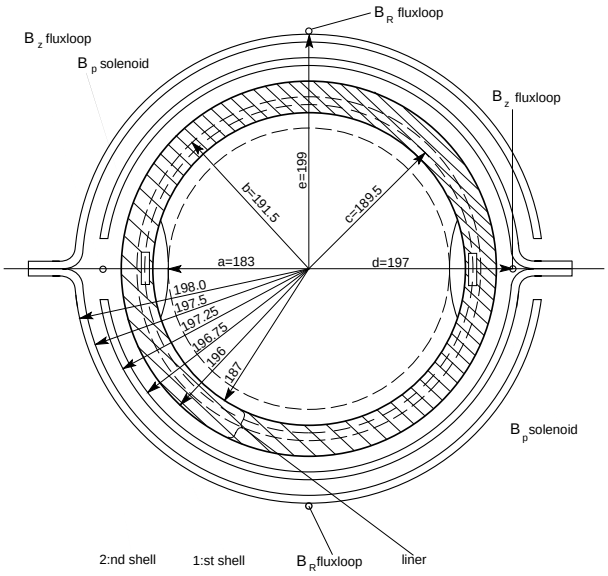

Figure 6: Sensor geometry

where r_{vf} and r_c are the minor radius where the saddle coil and the cosine coil are placed at respectively and

$$k_{p\,c} = \frac{\mu_0}{4\pi R_0}\left((1+\frac{a^2}{r_c^2})(\ln\frac{8R_0}{a}-1)+\ln\frac{a}{r_c}+1\right)$$

$$k_{p\,vf} = \frac{\mu_0}{4\pi R_0}\left((1-\frac{a^2}{r_{vf}^2})(\ln\frac{8R_0}{a}-1)+\ln\frac{a}{r_{vf}}\right)$$

$$k_{zc} = (1+\frac{a^2}{r_c^2})$$

$$k_{zvf} = (1-\frac{a^2}{r_{vf}^2})$$

The equation for the control variable xI_1 can be written

$$xI_1 = a_\Xi B_{cos} + b_\Xi B_{vf} + c_\Xi I_1 \tag{26}$$

To extract xI_1 from sensor data it would be necessary to implement and calibrate an analog equivalent circuit to perform the three multiplications and additions.

If Λ is chosen as the second variable instead, the matrix equation takes the following form:

$$\begin{bmatrix} -\frac{\mu_0}{2\pi r_c^2} & k_{\Lambda c} \\ \frac{\mu_0}{2\pi r_{vf}^2} & k_{\Lambda vf} \end{bmatrix} \begin{bmatrix} xI_1 \\ \Lambda I_1 \end{bmatrix} = \begin{bmatrix} B_{cos} \\ B_{vf} \end{bmatrix} - \begin{bmatrix} k_{\Lambda p\, c} \\ k_{\Lambda pvf} \end{bmatrix} I_1 \tag{27}$$

with

$$k_{\Lambda p\, c} = \frac{\mu_0}{4\pi R_0}\left(\ln\frac{r_c}{a} - 1 + \frac{1}{2}(1+\frac{a^2}{r_c^2})\right)$$

$$k_{\Lambda p\, vf} = \frac{\mu_0}{4\pi R_0}\left(\ln\frac{r_{vf}}{a} + \frac{1}{2}(1-\frac{a^2}{r_{vf}^2})\right)$$

$$k_{\Lambda c} = -\frac{\mu_0}{4\pi R_0}(1+\frac{a^2}{r_c^2})$$

$$k_{\Lambda vf} = -\frac{\mu_0}{4\pi R_0}(1-\frac{a^2}{r_{vf}^2})$$

Solving for Λ we get

$$\Lambda I_1 = a_\Lambda B_{cos} + b_\Lambda B_{vf} + c_\Lambda I_1 \tag{28}$$

3.3 Extraction of magnetic noise

As can be seen above, Λ can be calculated in the same way as xI_1. δB_z however requires additional analysis. B_z^{ext} contains all vertical field components (shell, OH, vf-coils...) except that from the plasma itself. We can write

$$B_z^{ext} = B_z^{OH} + B_z^{shell} + B_z^{vf} + \delta B_z$$

where δB_z is a disturbance field. Apart from δB_z, all of these field components can be calculated or measured directly. That makes it possible to estimate the magnetic noise and compensate for it through feed-forward control.

The components of B_z^{ext} are:

$$B_z^{OH} = -B_{e0}\frac{I_1}{I_0}\left(\frac{R}{R_0}\right)^m \approx -B_{e0}\frac{I_1}{I_0}(1+m\frac{x}{R_0}) = -\frac{B_{e0}}{I_0}I_1 - \frac{B_{e0}m}{R_0 I_0}\Xi \tag{29}$$

B_{e0} is the equilibrium vertical field $B_{e0} = \frac{\mu_0 I_0 \Gamma_0}{4\pi R_0}$

$$\hat{B}_z^{shell} = \frac{\mu_0}{4b}\hat{I}_2 = -\frac{\mu_0 s}{4bR_2}\left[\left(\frac{2L_{22}}{\pi b} + \frac{\pi b\Omega_F^2 M}{2I_0^2}\right)\hat{\Xi} + (\pi^2 bR_0 - D_{2B})\delta\hat{B}_z\right] = \\ = -sm_{12}\,\hat{\Xi} \tag{30}$$

Here the contribution from I_3 has been eliminated using equations 11. The factor in front of $\delta\hat{B}_z$ is zero for a homogeneous field.

$$B_z^{vf} = \frac{\mu_0}{\pi}\left(\frac{x_2}{x_2^2+y_2^2} - \frac{x_1}{x_1^2+y_1^2}\right) I_3 = g_3 I_3 \tag{31}$$

See figure 26 for geometry.

In summary

$$\delta\hat{B}_z = \hat{B}_z^{ext} + \frac{B_{e0}}{I_0}\hat{I}_1 - g_3\hat{I}_3 + (m_{12}s + \frac{B_{e0}m}{R_0 I_0})\,\hat{\Xi} \tag{32}$$

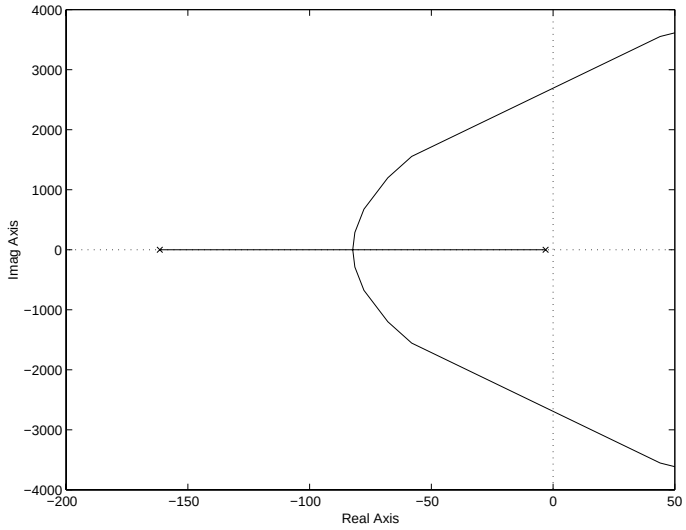

Figure 7: Root locus plot of $WG(s)$ for $T = 20\ \mu s$ ($f_{PS} = 25kHz$)

4 The controller

4.1 Model stability

If only the plasma-shell model is considered it will be a simple second order system. The power supply lowers the phase margin at higher frequencies. Additional poles and zeros may be present, but are unaccounted for. This adds up to a transfer function of the form

$$WG(s) = \frac{Ke^{-Ts}}{(1 + \frac{s}{\omega_1})(1 + \frac{s}{\omega_2})} \tag{33}$$

with $\frac{1}{T} \gg \omega_1, \omega_2$. The closed loop system (without controller) becomes

$$G_{CL}(s) = \frac{WG}{1 + WG} = \frac{Ke^{-Ts}}{(1 + \frac{s}{\omega_1})(1 + \frac{s}{\omega_2}) + Ke^{-Ts}} \tag{34}$$

In a root locus plot the poles of the closed system are plotted as a function of system gain K. The stability requirement is that all poles are located in the left half plane. As can be seen in figure 7 the system is stable as long as the gain is small. The non-linearity presented by the limited power supply output also degrades stability but has to be modelled in `simulink`.

How far the system is from instability is also of interest. The phase margin is a measure of this. It is defined as the amount the phase curve in a bode diagram could drop before reaching $-180°$ at the point where the amplitude curve cuts 0 dB (see figure 8). If the system amplification were higher than 0 dB (1) for $-180°$ phase shift, instability would follow: A signal of the right frequency would be amplified and then returned by the negative feedback in phase, getting amplified again, and so on.

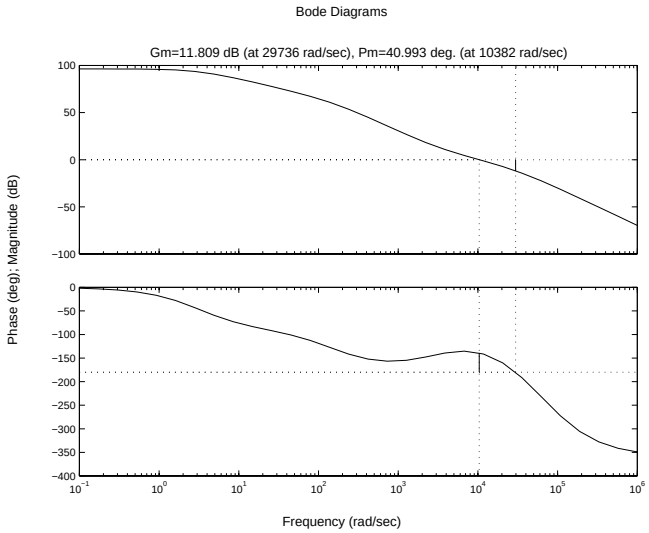

Figure 8: Phase and amplitude margin

The sensitivity function

$$S(s) = \frac{1}{1 + FWG(s)} \tag{35}$$

describes how well the system can handle model errors. It is a first order approximation of the transfer function from relative model error to relative output error. Section 6.3 in [2] contains a derivation of this expression. See figure 14 for typical appearance of this function. Low frequency model errors are well handled and at higher frequencies the shell should be able to compensate without help from the controller (figures 4 and 5 show the transfer functions of the disturbances).

4.2 PD controller

For a second order system the poles can be placed arbitrarily with a PID controller. This is not the case here, but at the cross-over frequencies of interest the system can be considered as a double integrator and a time delay. A PID controller is well suited to handle such problems.

The integrating (I) part of the PID removes stationary errors. In this case a small stationary error is of little importance and a fast settling time much more interesting. Losing the I-part also takes care of problems with integrator wind-up. Most of the controllers found in articles from other experiments (e.g. CLEO [3] and ISX-B [1]) were of the PD type.

Using derivative action presents other difficulties. A pure PD controller is impossible to construct in practice. It would require an infinitely high amplification for (infinitely) fast changing error signals. High frequency measurement noise would drown the control signal completely. So it is necessary to have some

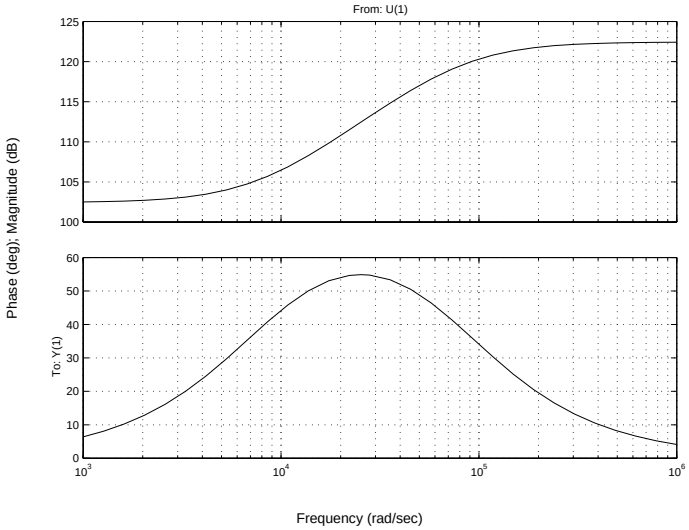

Figure 9: Bode diagram of realistic PD controller

sort of low-pass filtering. The realistic PD controller is modelled as

$$F(s) = K_p \frac{1 + sT_D}{1 + s\frac{T_D}{N}} = \frac{K_p}{N} \frac{s + \omega_D}{s + N\omega_D} \tag{36}$$

The factor N is chosen as high as possible to get a good derivative approximation while still providing adequate high frequency rejection. Usually $N \sim 10$.

4.3 Parameter optimization

The objective is to have the fastest system for given values of phase margin φ_m and T. That corresponds to finding as large cross-over frequency ($|G_{OL}(i\omega_c)| = 1$) as possible while still having sufficient phase margin.

Starting from the open-loop transfer function

$$G_{OL}(s) = \frac{KK_p}{N} \frac{e^{-Ts}}{(1 + \frac{s}{\omega_1})(1 + \frac{s}{\omega_2})} \frac{s + \omega_D}{s + N\omega_D} \tag{37}$$

the plasma-shell dynamics (ω_1, ω_2) can be approximated as a double integrator in the range of interesting cross-over frequencies.

$$G_{OL}(s) \approx \frac{\omega_1\omega_2 KK_p}{N} \frac{s + \omega_D}{s^2(s + N\omega_D)} e^{-Ts} \tag{38}$$

Taking the argument

$$\arg G_{OL}(i\omega) = \arctan \frac{\omega}{\omega_D} - T\omega - \pi - \arctan \frac{\omega}{N\omega_D} \tag{39}$$

Resulting in a phase margin

$$\varphi_m = \arg G_{OL}(i\omega) + \pi = \arctan \frac{\omega}{\omega_D} - \arctan \frac{\omega}{N\omega_D} - T\omega \tag{40}$$

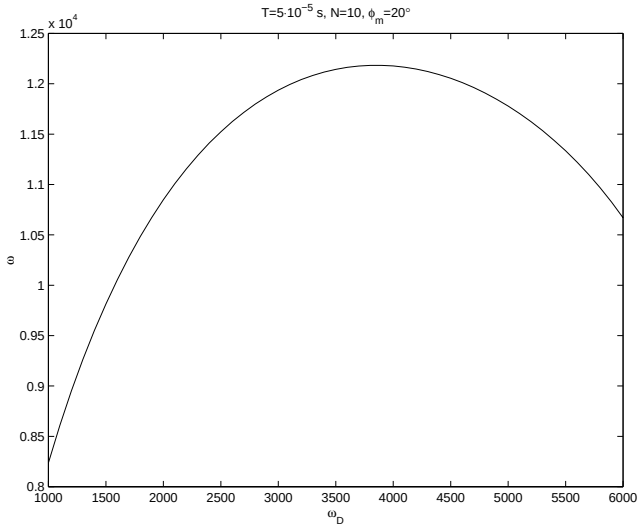

Figure 10: $\omega(\omega_D)$ for constant φ_m and T

For constant φ_m and T the phase margin equation becomes a function $\omega(\omega_D)$. This function has a maximum (see figure 10), so the derivative with respect to ω_D is taken of equation 40.

$$\frac{d}{d\omega_D} \Rightarrow \; -\left(\frac{\omega}{\omega_D^2} - \frac{1}{\omega_D}\frac{d\omega}{d\omega_D}\right)\frac{1}{1+\frac{\omega^2}{\omega_D^2}} + \left(\frac{\omega}{N\omega_D^2} - \frac{1}{N\omega_D}\frac{d\omega}{d\omega_D}\right)\frac{1}{1+\frac{\omega^2}{N^2\omega_D^2}} - T\frac{d\omega}{d\omega_D} = 0 \quad (41)$$

$\frac{d\omega}{d\omega_D} = 0$ at the maximum.

$$-\frac{\omega}{\omega_D^2+\omega^2} + \frac{N\omega}{N^2\omega_D^2+\omega^2} = 0 \quad (42)$$

$$\Rightarrow \frac{\omega}{\omega_D} = \sqrt{\frac{N^2-1}{N-1}} = \sqrt{N+1} \quad (43)$$

Inserting this into the phase margin equation gives

$$\varphi_m = \arctan\sqrt{N+1} - \arctan\sqrt{\frac{N+1}{N^2}} - T\omega \quad (44)$$

and

$$\omega = \left(\arctan\sqrt{N+1} - \arctan\sqrt{\frac{N+1}{N^2}} - \varphi_m\right)\frac{1}{T} \quad (45)$$

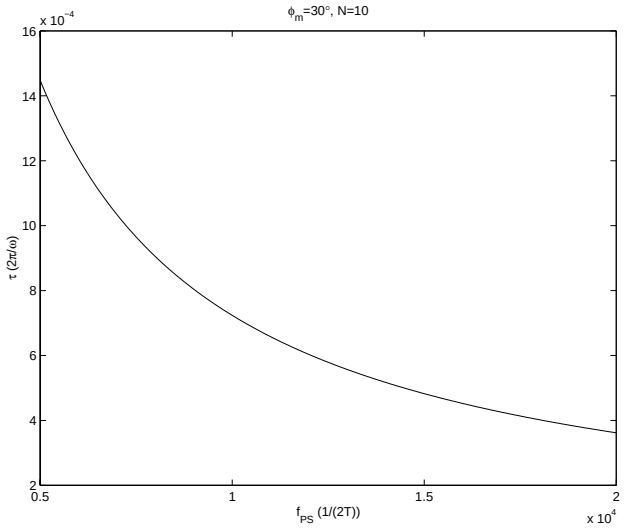

Figure 11: Controller settling time as a function of power supply switching frequency

By choosing an appropriate controller gain, the system cross-over frequency ω_c can be set to coincide with ω.

$$|G_{OL}(i\omega_c)|^2 = \frac{\omega_1^2\omega_2^2K^2K_p^2}{N^2}\frac{\omega_c^2+\omega_D^2}{\omega_c^4(\omega_c^2+N^2\omega_D^2)} = \frac{\omega_1^2\omega_2^2K^2K_p^2}{N^2}\frac{1+\frac{1}{N+1}}{\omega_c^4(1+\frac{N^2}{N+1})} =$$

$$= \frac{\omega_1^2\omega_2^2K^2K_p^2}{N^2}\frac{N+2}{\omega_c^4(N^2+N+1)} = 1 \;\Rightarrow\; K_p = \frac{N}{\omega_1\omega_2K}\omega_c^2\sqrt{\frac{N^2+N+1}{N+2}} \quad (46)$$

In summary the controller parameters are determined as follows.

$$\omega_D = \frac{1}{\sqrt{N+1}}\left(\arctan\sqrt{N+1} - \arctan\sqrt{\frac{N+1}{N^2}} - \varphi_m\right)\frac{1}{T} \quad (47)$$

$$K_p = \frac{N}{\omega_1\omega_2K}\sqrt{\frac{N^2+N+1}{N+2}}\left(\arctan\sqrt{N+1} - \arctan\sqrt{\frac{N+1}{N^2}} - \varphi_m\right)^2\frac{1}{T^2} \quad (48)$$

4.4 Feed forward

If a disturbance can be measured and modelled its effect on the output signal can be eliminated or at least reduced through feed forward. See figure 12 for a block diagram of the situation. The main advantage of feed forward is that it counters the disturbance before it shows up on the output. In optimal conditions the feed forward link can be set as

$$F_f = -\frac{H}{G_{OL}} \quad (49)$$

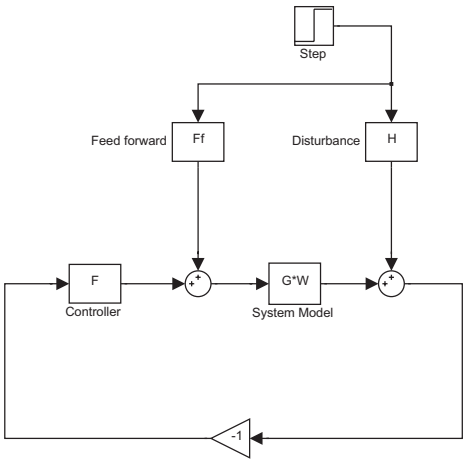

Figure 12: Feed forward

and completely eliminate the disturbance. However, the time delay in the power supply would require a non-causal transfer function e^{sT} and has to be omitted. In EXTRAP perturbations in Λ and δB_z can, theoretically, be subjected to feed forward reduction. When calculating the link $F_f(s)$ for $G_\Lambda(s)$ and $G_B(s)$ it is found that some form of derivation is required (double derivation in the case of Λ). Consequently $F_f(s)$ has to be approximated in the same way as the PD controller.

5 Results

5.1 Settling time

The specifications for the controller call for a settling time of less than 1 ms to a step load disturbance while still keeping a reasonable stability margin ($\varphi_m \geq 30°$). Equation 45 gives a rough estimate of how the speed of the system depends on T and φ_m (and N). Comparison with simulations in `simulink` show that it agrees quite well. Controller parameters ω_D and K_p are then obtained using equations 47 and 48. These would be good starting values for tuning the controller. Numerically, ω_D is in the order of 10^3 and $K_p \sim 10^2$. A minimal switching frequency realizing the design goals is 7.5 kHz (cf figure 11). Increasing the switching frequency further will result in a higher phase margin and/or faster system. Typical step response curves for $f_{PS} = 7.5$ kHz and 20 kHz can be seen in figure 13.

5.2 Noise rejection

The sensitivity function $S(s)$ (figure 14) indicates how well the system can suppress noise. Higher frequencies have much worse disturbance rejection. The amplitude curve levels off at around $\omega = 10^6$ rad/s. Two different types of disturbances are discussed here, Λ and δB_z. In addition to these two, measurement noise can be a problem.

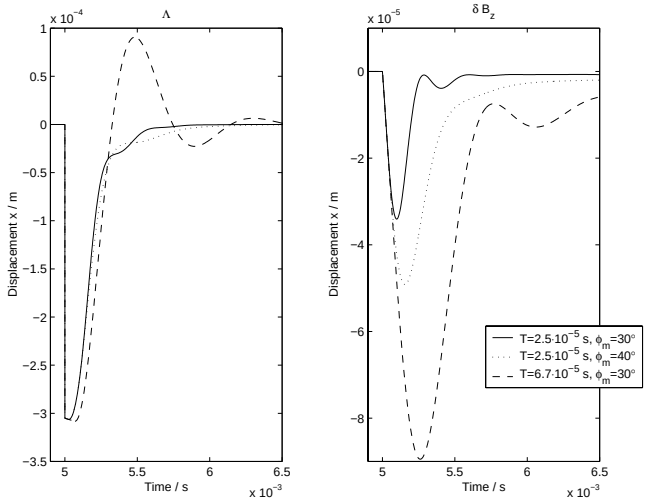

Figure 13: Response to a 0.01 step in Λ and 2 mT step in δB_z for a few parameter choices. $V_{max} = 1.6$ kV and $N = 10$ for these plots.

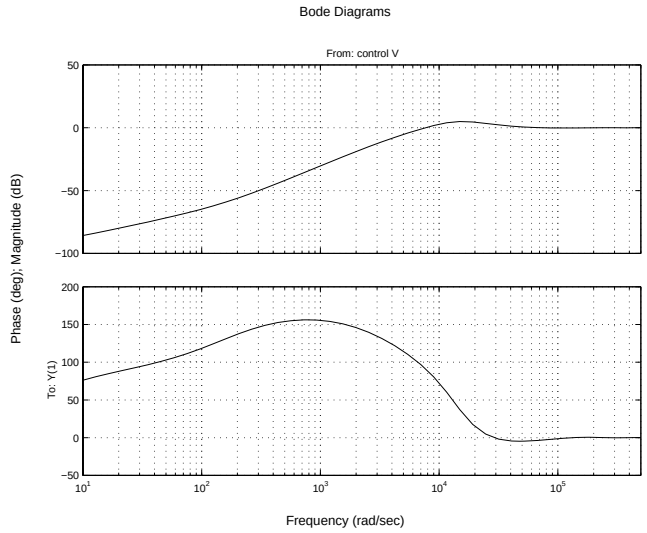

Figure 14: Sensitivity function. Parameters: $T = 2.5 \cdot 10^{-5}$ s, $\varphi = 40°$ and $N = 10$

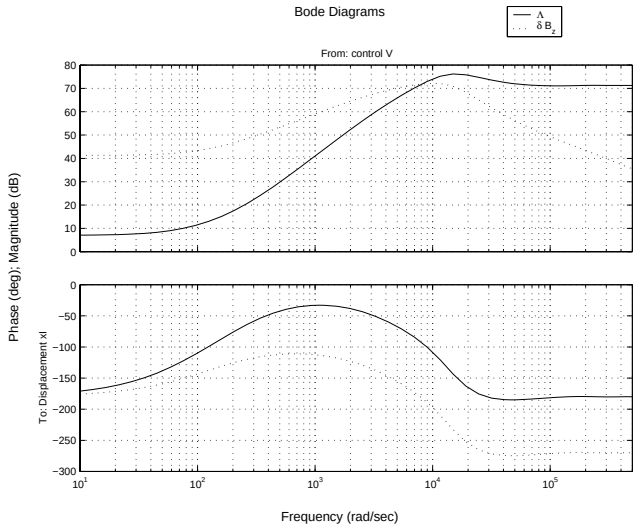

Figure 15: Disturbance closed loop transfer function. Parameters: $T = 2.5 \cdot 10^{-5}$ s, $\varphi = 40^\circ$ and $N = 10$

The switching power supply generate high frequency ripple, but it will be effectively filtered by the vf-coils and copper shell. Practically nothing will penetrate to move the plasma.

The transfer function from some sort of fluctuation to plasma displacement (see block diagram in figure 2) is given by

$$G_\delta \cdot S(s) \tag{50}$$

Figure 15 shows this function for Λ and δB_z. By far the hardest to control, disturbances in Λ cause the plasma to move instantly (inertia neglected). A reconfiguration of the plasma radial profile due to e.g. changes in current density is the source of these disturbances. The current density changes could be caused by influx of particles from the wall, cooling the plasma edge and increasing its resistivity.

In contrast, δB_z-disturbances are quite easy to control because of the low-pass filtering of the copper shell. Variations in currents in external coils cause fluctuations in the vertical magnetic field.

Measurement noise is typically "white noise" picked up wires or produced by electrical components and contains high frequency components. This will result in plasma movement as the controller responds with false control signals. Since the D-part of the controller amplifies transients, the high frequency contents are the most problematic. Low-pass filtering the signal before feeding it to the controller will reduce the problem. A cut-off frequency about a decade higher than $N\omega_D$ would be sufficient.

5.3 Saturation

To see the effect of saturation a step load disturbance δB_z of increasing amplitude was simulated. When the power supply starts to saturate (around

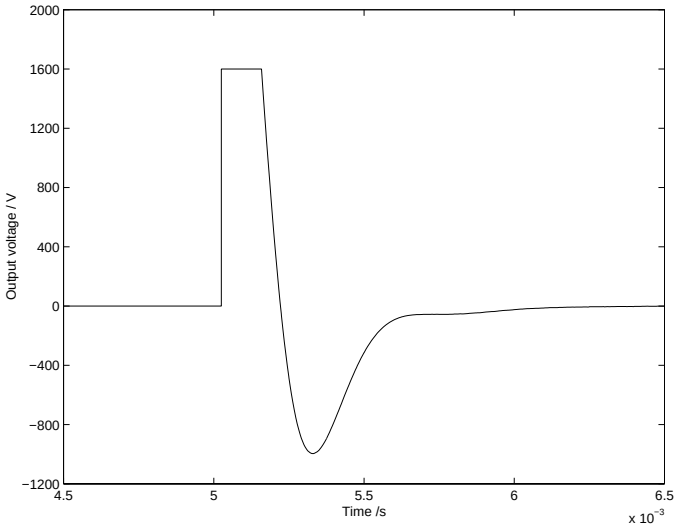

Figure 16: Power supply saturated output in response to a 0.025 step in Λ. $T = 2.5 \cdot 10^{-5}$ s, $\varphi_m = 40°$ and $N = 10$ for this plot.

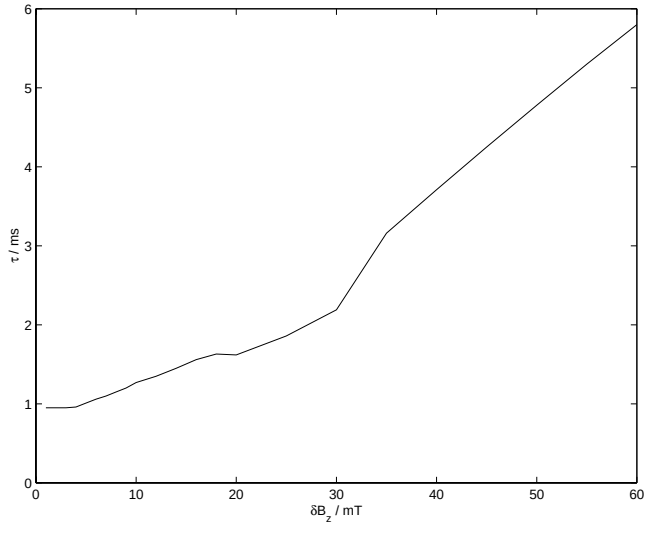

Figure 17: τ for increasing δB_z

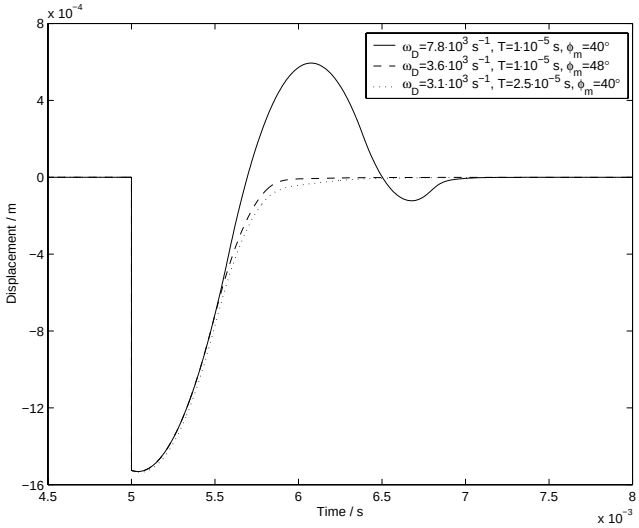

Figure 18: Fast controller saturation. Additional data for this plot: $V_{max} = 800$ V and $N = 10$. The step in Λ was 0.05.

$\delta B_z = 4$ mT in figure 17), the settling time goes up. The plot looks irregular because of over-shoot effects that go above or below the 95 % level defining the settling time.

With a PD controller, transients generate very large control signals saturating the power supply. Λ-noise is much more troublesome than δB_z, as its transfer function only damps, not filters, high frequencies. Also, a slower controller is less likely to saturate. A fast system (small T and large ω_D) without voltage capabilities to match it can do more harm than good, see figure 18. It is better to use a large switching frequency (small T) to increase the phase margin.

If IGBT:s are used as driving components in the power supply the maximum output voltage will be around 800 V. If two are connected in series, $V_{max} = 1600$ V instead. Currents flowing in the control coil can then reach 2 kA. Testing with these two alternatives figure 19 was created. It shows the disturbance level at which the settling time has increased by 10 % due to saturation. The disturbance was modelled as a step in Λ of amplitude $\delta\Lambda$. Clearly a slower controller (corresponding to longer switching time T in the figure) can handle higher amounts of noise before saturating.

5.4 Feed forward

Simulations with feed forward control appear to show that it would have little or no effect on the overall performance. Some sort of approximation is necessary because of the resulting pure derivatives and the time delay in the power supply. In the case of magnetic fluctuations improvement can still be seen with feed forward (figure 20). But for the dominating source of plasma displacement noise, Λ, there seems to be no improvement. The reason for this could be that a fluctuation is immediately visible as plasma movement. The feed forward link

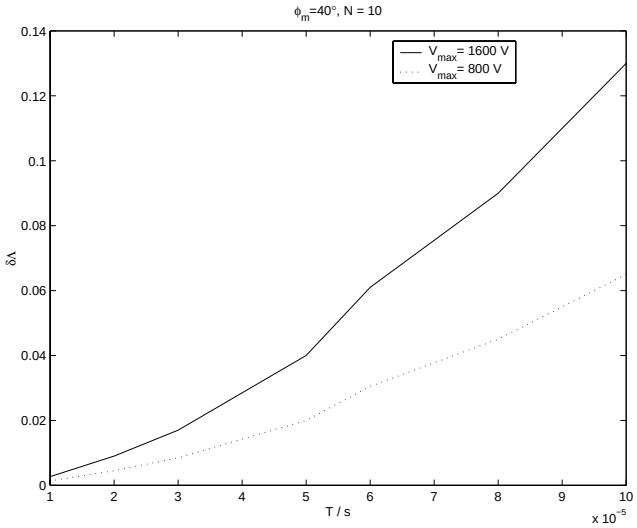

Figure 19: Saturation levels for different configurations

cannot compensate for the fluctuation before it appears as a displacement.

5.5 Real data

Sensor data from earlier experiments was used to test the controller. Signals from cosine coil, vertical flux sensor and Rogowski coil was combined to extract Λ and magnetic noise δB_z during the shot (see figure 21).

Without feedback control the plasma drifted radially up to a centimeter (figure 22). What the sensors actually measure is xI_1 and that has to be divided by I_1 to get the displacement x. The strange values at the start and end of the shot are explained by this, as the plasma current I_1 is near zero there.

With the noise data as input, feedback control was simulated. The displacement was effectively reduced by the controller to less than a millimeter (figure 22). The simulation parameters for this plot are $T = 2.5 \cdot 10^{-5}$ s, $V_{max} = 1.6$ kV and $\varphi = 40°$. As can be seen in figure 23 the power supply is highly saturated most of the time. A maximum output voltage of around 5 kV would have been needed to avoid saturation. A faster system would benefit more from higher output voltage, see figure 24.

6 Conclusions

The plasma radial position can be controlled with a PD controller and pulse width modulated power supply. Equations 47 and 48 should give good starting values for tuning the controller.

As for the power supply, increasing the switching frequency enables faster control or greater phase margin (stability). To achieve minimum specifications, $\tau = 1$ ms and $\varphi_m = 30°$, a switching frequency $f_{PS} > 7.5$ kHz is required. If

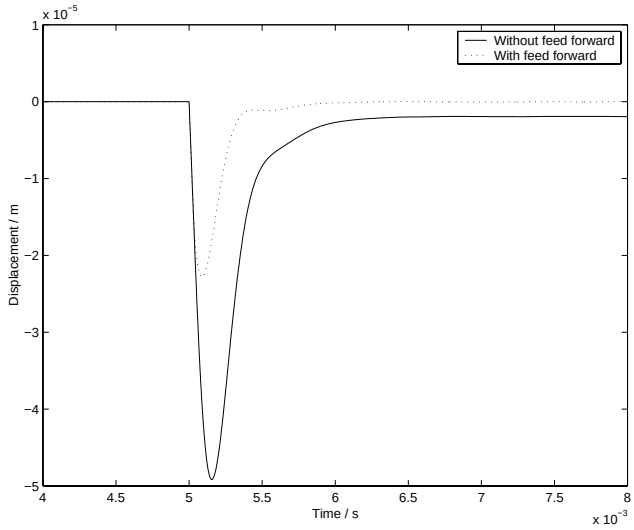

Figure 20: Displacement with and without feed forward

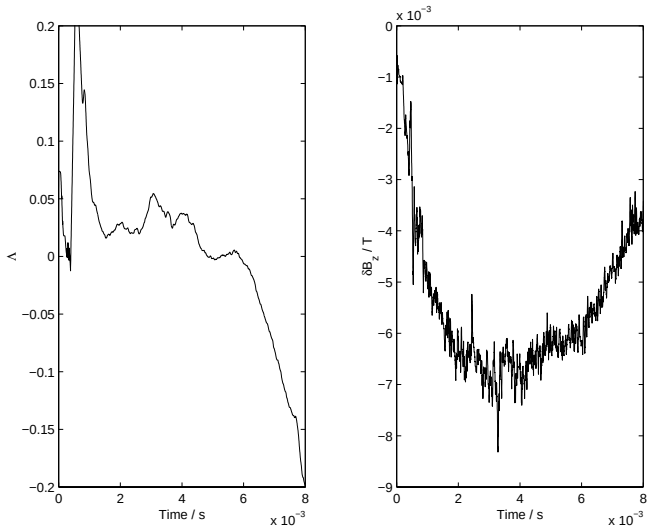

Figure 21: Fluctuations in Λ and δB_z during shot 3583

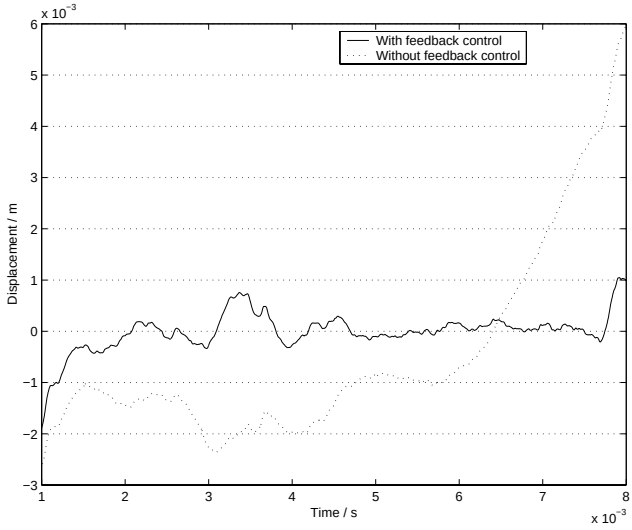

Figure 22: Displacement with and without feedback control (shot 3583)

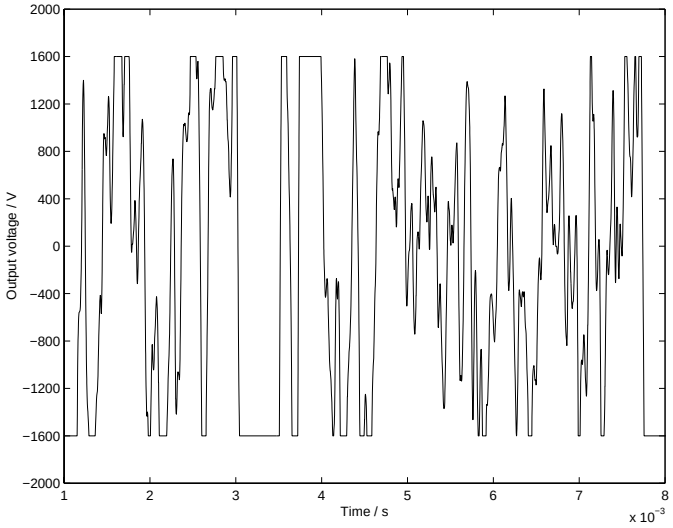

Figure 23: Output voltage during control (shot 3583)

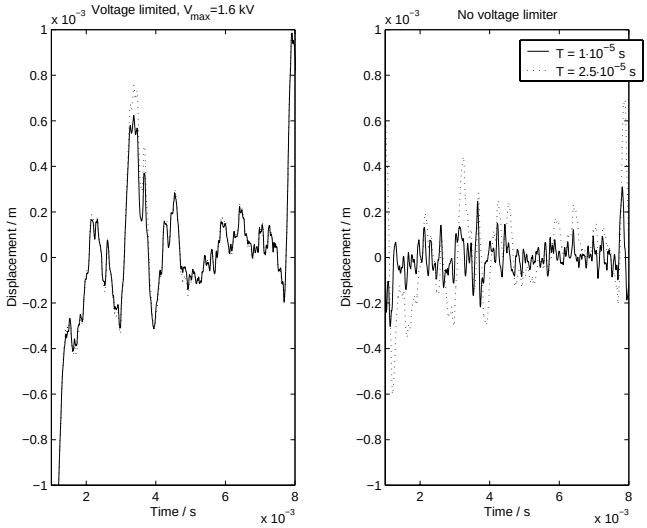

Figure 24: Displacement for different switching frequencies with and without voltage limiter (shot 3583, $\varphi_m = 40°$)

f_{PS} is increased to 20 kHz, a settling time of just over 0.5 ms can be obtained with a phase margin of 40°.

Saturation increases the settling time and is an issue for Λ noise. A maximum output voltage of 800 V could prove too small to combat disturbances in Λ. Another effect of saturation is that it might not be best to use the fastest possible controller. It would require large output voltages and saturate easily. A better solution would be to settle for a slower controller but with a higher phase margin.

Acknowledgements

The author wishes to thank his supervisors, Docent P. Brunsell (KTH) and Professor P. Hagander (LTH), for all their help. The work done by R. Kalinowski in drawing the geometrical figures is also very much appreciated.

A Notation

A hat ($\hat{}$) denotes a Laplace transformed variable. Index 0 generally stands for an equilibrium state and 1,2,3 for plasma, shell, control coils respectively. δ represents a small perturbation. The following symbols are used throughout the text:

b	Shell minor radius
a	Plasma minor radius
R_0	Plasma equilibrium major radius
R	Plasma major radius
x	Plasma radial displacement $(R - R_0)$
M	Mass of a plasma ion
m	External vertical field gradient $(\frac{dB_z}{dR}\frac{R}{B_z})$
Ω_F	Plasma oscillation frequency in vertical field
Λ	Plasma asymmetry parameter
Γ	$\ln(\frac{8R}{a}) - \frac{1}{2} + \Lambda$
B_{ze}	Equilibrium field for the actual plasma parameters
B_z^{OH}	Vertical magnetic field from Ohmic heating transformer
B_z^{shell}	Vertical magnetic field from induced currents in the copper shell
B_z^{vf}	Vertical magnetic field from control coils
B_z^{ext}	Vertical magnetic field by external sources (not plasma)
δB_z	Disturbance in the vertical magnetic field
B_{vf}	Average vertical magnetic field (measured by sensor)
B_{cos}	First harmonic poloidal magnetic field (measured by sensor)
I_0	Plasma equilibrium current
I_1	Plasma current
I_2	Total current flowing in one half of the shell
I_3	Control current
V	Control voltage
L_{12}	Mutual inductance between plasma and shell
L_{13}	Mutual inductance between plasma and control coils
L_{22}	Shell self inductance
L_{23}	Mutual inductance between shell and control coils
L_{33}	Control coils self inductance
R_2	Shell resistance
R_3	Control coils resistance
Ξ	xI_1 (control variable)
$\mathtt{x}$	A vector $[\Xi\ I_2\ I_3]^T$
ω_1	Plasma-shell dynamics first pole
ω_2	Plasma-shell dynamics second pole
f_{PS}	Power supply switching frequency
T	Half of the power supply switching time $(\frac{1}{2f_{PS}}) \sim 10 - 60\ \mu s$

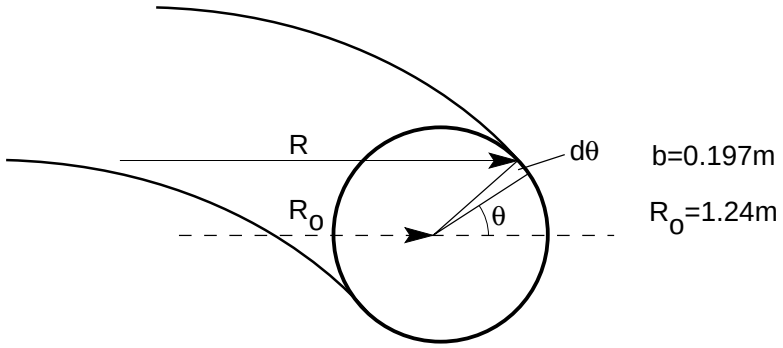

Figure 25: Geometry L_{22}

G	Control voltage $\hat{V}$ to plasma displacement $\hat{\Xi}$ transfer function
G_Λ	Perturbation in parameter $\delta\hat{\Lambda}$ to plasma displacement $\hat{\Xi}$ transfer function
G_B	Magnetic perturbation $\delta\hat{B}_z$ to plasma displacement $\hat{\Xi}$ transfer function
W	Power supply transfer function
F	Controller transfer function
F_f	Feed forward transfer function
G_{OL}	Open-loop transfer function (FWG)
G_{CL}	Closed-loop transfer function ($\frac{FWG}{1+FWG}$)
T_D	PD controller derivative time
ω_D	$\frac{1}{T_D}$
K_p	PD controller gain
N	PD controller derivative cut-off factor
φ_m	Phase margin
τ	Settling time (95 % of final value)
ω_c	Cross-over frequency ($\lvert G_{OL}(i\omega_c)\rvert = 1$)

B Inductances

A large aspect ratio approximation ($\frac{R_0}{b} \gg 1$) will be used in all of the following calculations. That means toroidal effects are neglected and the vacuum vessel can be considered as a cylinder.

B.1 L_{22}

The shell is assumed to carry a current varying as $di(\theta) = \frac{I_2}{2}\cos\theta\, d\theta$. This produces a vertical homogeneous magnetic field inside the vacuum vessel. The contribution from current element $di(\theta)$ to the vertical part of the magnetic field in the center is:

$$dB_z = \frac{\mu_0}{2\pi b} di(\theta)\cos\theta \tag{51}$$

Integration gives the field:

$$B_z = \int_0^{2\pi} \frac{\mu_0}{4\pi b} I_2 \cos^2\theta\, d\theta = \frac{\mu_0}{4b} I_2 \tag{52}$$

In order to calculate the inductance, the shell is divided into infinitesimal circular elements that has a certain loop voltage. Each loop encloses a magnetic flux (see figure 25):

$$\Phi(\theta) = \iint \mathbf{B} \cdot d\mathbf{S} = \pi R^2 B_z = \pi(R_0 + b\cos\theta)^2 B_z \tag{53}$$

The magnetic field is not B_z outside the shell, but for every current element $di(\theta)$ there is a corresponding element $-di(\theta)$ at the same height, so the outside won't contribute to the flux.

According to Faraday's law the induced loop voltage is:

$$v = \oint \mathbf{E} \cdot d\mathbf{l} = -\iint \frac{\partial \mathbf{B}}{\partial t} \cdot d\mathbf{S} = -\frac{\partial \Phi}{\partial t} \tag{54}$$

Power in an element (directions defined so that the power is positive):

$$\begin{aligned} dp = v\, di = v\frac{I_2}{2}\cos\theta\, d\theta = \\ = \pi(R_0 + b\cos\theta)^2 \frac{\partial B_z}{\partial t}\frac{I_2}{2}\cos\theta\, d\theta = \frac{\mu_0 \pi}{8b}(R_0 + b\cos\theta)^2 \cos\theta\, I_2 \frac{\partial I_2}{\partial t}\, d\theta \end{aligned} \tag{55}$$

The total power flowing in the shell becomes:

$$\begin{aligned} P = \int_0^{2\pi} \frac{\mu_0 \pi}{8b}(R_0 + b\cos\theta)^2 \cos\theta\, I_2 \frac{\partial I_2}{\partial t}\, d\theta = \\ = \frac{\mu_0 \pi^2 R_0}{4} I_2 \frac{\partial I_2}{\partial t} = L_{22} I_2 \frac{\partial I_2}{\partial t} \end{aligned} \tag{56}$$

And the inductance can be identified as:

$$L_{22} = \frac{\mu_0 \pi^2 R_0}{4} \tag{57}$$

B.2 L_{23}

The calculation of L_{23} is pretty much the same as that for L_{22}, except that the magnetic field is generated by the control coils. Their field in the shell is approximately homogeneous and the value in the center is chosen (see figure 26 for geometry, the small circles are control coil windings):

$$B_z = \frac{\mu_0}{\pi}\left(\frac{x_1}{x_1^2 + y_1^2} - \frac{x_2}{x_2^2 + y_2^2}\right) I_3 \tag{58}$$

An average of the field over the midplane relative to the value at the center has been calculated for the Extrap T2 geometry,

$$\frac{B_{ave}}{B_{cen}} = 1.0061$$

justifying the homogeneous field approximation.

After integration of the total power, the inductance can be identified:

$$L_{23} = \mu_0 \pi b R_0 \left(\frac{x_1}{x_1^2 + y_1^2} - \frac{x_2}{x_2^2 + y_2^2}\right) \tag{59}$$

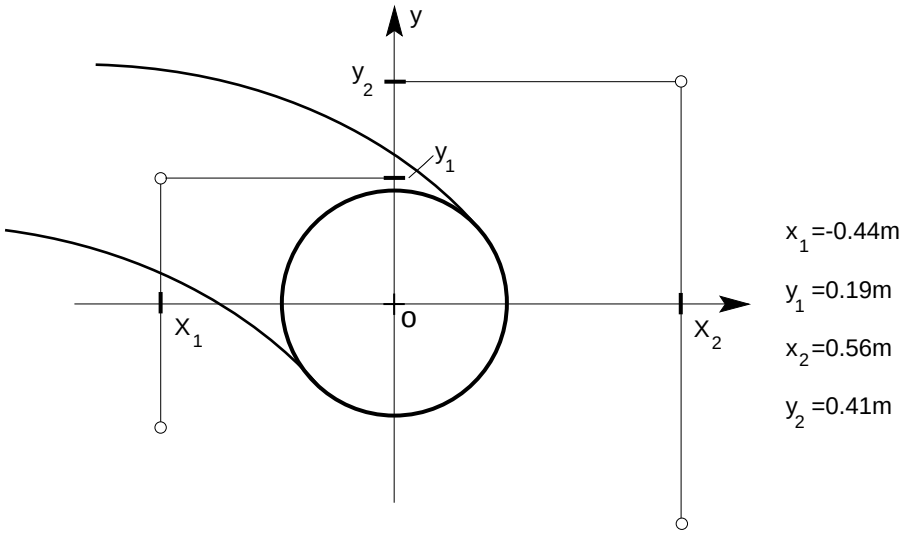

Figure 26: Geometry L_{23}

B.3 $\frac{dL_{12}}{dx}$

If the plasma major radius changes by dx, the change in enclosed flux is:

$$d\Phi = dA\, B_z(x) = 2\pi(R_0 + x)dx\, B_z(x) \tag{60}$$

where $B_z = \frac{\mu_0}{4b} I_2$ (see B.1).

$$\frac{dL_{12}}{dx} = \frac{1}{I_2}\frac{d\Phi}{dx} = \frac{2\pi(R_0 + x)B_z}{I_2} = \frac{\mu_0\pi(R_0 + x)}{2b} \tag{61}$$

The plasma displacement is assumed to be small compared to the major radius. Dropping terms in the order of $\frac{x}{R_0}$ and comparing with $L_{22} = \frac{\mu_0\pi^2 R_0}{4}$ results in:

$$\frac{dL_{12}}{dx} = \frac{2}{\pi b} L_{22} \tag{62}$$

Coupling between plasma and shell when the plasma current channel is centered is zero, so

$$L_{12} = \frac{2}{\pi b} x L_{22} \tag{63}$$

B.4 $\frac{dL_{13}}{dx}$

The calculation is similar to that for L_{12}, but the magnetic field is

$$B_z = \frac{\mu_0}{\pi}\left(\frac{x_1 - x}{x_1^2 + y_1^2} + \frac{x - x_2}{x_2^2 + y_2^2}\right) I_3$$

Consequently the derivative of the inductance can be written as:

$$\frac{dL_{13}}{dx} = 2\mu_0(R_0 + x)\left(\frac{x_1 - x}{x_1^2 + y_1^2} + \frac{x - x_2}{x_2^2 + y_2^2}\right) \tag{64}$$

Approximating $x \ll x_1, x_2, R_0$ and comparing with L_{23} (see B.2) gives:

$$\frac{dL_{13}}{dx} = \frac{2}{\pi b} L_{23} \tag{65}$$

and

$$L_{13} = \frac{2}{\pi b} x L_{23} \tag{66}$$

C Simulation tools

C.1 Matlab programs

There are many more or less empirical ways to find the right controller parameters (see e.g. [6]). Here Matlab's control toolbox has been used extensively. It allows you to specify transfer functions as polynomials and use normal operators (such as + and *) on them.

With `rltool` a model can be imported and its root locus plotted. Then the controller is constructed by adding poles and zeroes in the plot with the mouse. The gain can be set by selecting points in the root locus graph. The characteristics of the system (e.g. Bode diagram and step response) are updated in "real time" in another window.

To model feed forward and saturation of the power supply `simulink` was used. With it, noise could easily be injected at various points in the control loop. Blocks representing transfer functions and sources are simply connected and `simulink` then runs the simulation using an ode solver.

C.2 Matlab code

C.2.1 controlinit.m

Initialization file, run before starting `simulink`.

```
control2;
load transf9
load regulatorer2

H=tf(100/I0,1);

shot=3583

Bdistdata;
f2=tf(1,[1/(2*pi*2e3) 1])^3;
f=tf(1,[1/(2*pi*1e5) 1]);

feedforward;

T=1/(2*fps);
fim=40*pi/180;
N=10;
phasemargin4;
```

C.2.2 control2.m

Main m-file. Sets up all geometry data and transfer functions.

```
%
% model disturbance from external magnetic field Bext
% with only shell present
%

clear all


% physical constants:
%
% vacuum permeability
my0=4*pi*1e-7;

% experiment specific constants:
%
% control coil inboard position
x1=-0.44; y1=0.19;

% control coil outboard position
x2=0.56; y2=0.41;

% vacuum vessel radius
b=0.197;

% plasma minor radius
a=0.183;

% plasma mass
M=2e-8;

% equilibrium major radius
R0=1.24;

% equilibrium plasma current
I0=1.2e5;

% internal inductance per unit lenght
li=0.6;

% poloidal beta
betatheta=0.1;

% external vertical field gradient
m=-0.1;

% plasma current variation I~R^n
n=-0.2;

% copper shell time constant
tau2=5e-3;

% copper shell inductance
L22l=3.8448e-006; R2l=L22l/(tau2);

% shell-Bext mutual "inductance"
% from homogenous disturbance field
D2el=pi^2*R0*b;
```

```
L23l=2*pi*R0*L23*4; L33l=260e-6; R2l=L22l/(tau2);

R3l=20e-3; D3el=2*pi*(1.8^2-0.8^2);

% derived constants

Gamma0=log(8*R0/b)-3/2+li/2+betatheta;

Omegaf2=my0*I0^2*((1+m)*Gamma0-1/2)/(2*R0*M);
% Omegaf2=my0*I0^2*((1+m)*Gamma0-(1-R0/a))/(2*R0*M);

% Useful transfer functions
shell=tf([L22l R2l],1); der=tf([1 0],1);


%
% model transfer function
%



cp2=M*Omegaf2*pi^2*b^2; es=4*I0^2*L22l;


% Plasma transfer function
q0=2*L23l*R2l*pi*b*I0^2; p0=cp2*R2l*R3l;
p1=cp2*(L22l*R3l+L33l*R2l)+4*I0^2*(L22l^2*R3l+L23l^2*R2l);
p2=(cp2+es)*(L22l*L33l-L23l^2); G=tf(q0,[p2 p1 p0]); zpk(G)
set(G,'inputn','control V','outputn','Displacement xI');

% Control coil transfer function
q1=4*L22l^2*I0^2+M*Omegaf2*pi^2*b^2*L22l;
q0=M*Omegaf2*pi^2*b^2*R2l;
p2=-4*L22l*I0^2*L23l^2+4*L22l^2*I0^2*L33l
    +M*Omegaf2*pi^2*b^2*L22l*L33l-M*Omegaf2*pi^2*b^2*L23l^2;
p1=4*L22l^2*I0^2*R3l+4*L23l^2*R2l*I0^2
    +M*Omegaf2*pi^2*b^2*L22l*R3l+M*Omegaf2*pi^2*b^2*R2l*L33l;
p0=M*Omegaf2*pi^2*b^2*R2l*R3l; J = tf([q1 q0],[p2 p1 p0]); zpk(J)
set(J,'inputn','control V','outputn','control I');

% Xi -> I2 transfer function
S1=2*L22l*der/(pi*b*shell);

% I3 -> I2 transfer funciton
S2=L23l*der/shell;

% Vertical flux sensor transer functions
% (assuming ideal integration after the flux loops)
M1=tf(2*my0*(R0-b)/b); M2=tf(pi*my0);
M3=tf(4*my0*b*(x2/(x2^2+y2^2)-x1/(x1^2+y1^2)));

% Power supply transfer function
% (modelled as time delay)
fps=2e4;            % cut-off frequency
W2=tf(1,1,'iodelaymatrix',1/(2*fps)); set(W2,'inputn','control
signal','outputn','control V');
W3=pade(W2,1);  % First order Pade approximation of time delay
set(W3,'inputn','control signal','outputn','control V');


% transfer function for vertical field disturbance
```

```
% with control coil and shell
a1=2*L22l/(pi*b)+pi*b*Omegaf2*M/(2*I0^2);
a2=2*L23l/(pi*b)+pi*b*Omegaf2*M*L33l/(L23l*2*I0^2);
b2=pi*b*Omegaf2*M/(2*I0^2); c1=L23l-L33l*L22l/L23l;
d1=pi^2*b*R0-D2el; d2=pi^2*b*R0*L33l/L23l-D3el;

G4=-tf([-d1*c1/R2l d2+R3l*L22l*d1/(R2l*L23l)
pi^2*b*R0*R3l/L23l],[-a1*c1/R2l a2+R3l*L22l*a1/(R2l*L23l)
b2*R3l/L23l]); G5=tf(1,[-a1*c1/R2l a2+R3l*L22l*a1/(R2l*L23l)
b2*R3l/L23l]);

set(G4,'inputn','B fluctuation','outputn','Displacement xI');
set(G5,'inputn','control V','outputn','Displacement xI');

% transfer function for disturbance in lambda
% with control coil and shell
a2=L22l*L33l-L23l^2; a1=L22l*R3l+L33l*R2l; a0=R2l*R3l;
d1=M*Omegaf2*pi^2*b^2; d2=4*I0^2*L22l; p2=(d1+d2)*a2;
p1=d1*a1+d2*(L22l*R3l+L23l^2*R2l/L22l); p0=d1*a0;
G6=-my0*I0^3*pi^2*b^2*tf([a2 a1 a0],[p2 p1 p0]);

set(G6,'inputn','Lambda fluctuation','outputn','Displacement xI');
```

C.2.3 L23.m

Calculates the mutual inductance between the shell and the control coil.

```
function L23p=L23();

my0=4*pi*1e-7;

x1=0.44; y1=0.19; x2=-0.56; y2=0.41; b=0.25;

L23p=my0*b*(log(((b-x2)^2+y2^2)/((b+x2)^2+y2^2))
    +log(((b+x1)^2+y1^2)/((b-x1)^2+y1^2)))/(4*b*2)
```

C.2.4 Bdistdata.m

Extracts δB_z and Λ from measurement data. Λ is averaged over `Nm` data points and stored in `L2`.

```
%
% Calculation of disturbance part of Bz
% assumes Control2.m has already been run
%

my0=4*pi*1e-7;

x1=-0.44; x2=0.56; y1=0.19; y2=0.41;

b=0.197;            % copper shell radius

m=-0.1;             % OH-field gradient
```

```
g2=my0/(4*b); g3=my0*(x2/(x2^2+y2^2)-x1/(x1^2+y1^2))/pi;
m13=(2*L22l/(pi*b)+pi*b*Omegaf2*M/(2*I0^2))/R2l;

Be0=my0*I0*Gamma0/(4*pi*R0);        % equilibrium field

displacement;

xI2=zeros(size(xI,1),1);
xI2(2:size(xI,1)-1)=(xI(2:size(xI,1)-1)+xI(1:size(xI,1)-2)
    +xI(3:size(xI,1)))/3;

dXi=diff(xI2)/dtmin; dXi=[0 dXi'];
dB=Bz+pla_ny'*Be0/I0+m13*g2*dXi'+Be0*m*xI/(R0*I0);

Lambda=0.5-log(8*R0/a)-4*pi*R0*Bz./(pla_ny'*my0);
lone=ones(size(Lambda)); Lambda=min(Lambda,lone*0.5);
Lambda=max(Lambda,-lone);

Nm=351;
L2=zeros(size(Lambda,1),1);
for j=500:size(Lambda,1)-Nm
   L2(j+round(Nm/2))=sum(Lambda(j:j+Nm))/Nm;
end
```

C.2.5 displacement.m

Calculates the plasma displacement x from experimental data in shot number `shot`.

```
%
% This m-file calculates the displacement
% from experimental measurements
% of vertical field and cosine component
% of the poloidal field.
%

[t dtmin pla_ny cos_ny ver_ny]=conformdata2(shot);

% physical constants:
% vacuum permeability
my0=4*pi*1e-7;

% experiment specific constants:
%
% plasma minor radius
a=0.183;
% equilibrium major radius
R0=1.24;
% cosine coil radius
rc=0.1895;
% saddle coil radius
rs=0.197;
%
% constant definitions
%

kpc=my0*((1+a^2/rc^2)*(log(8*R0/a)-1)+log(a/rc)+1)/(4*pi*R0);
kps=my0*((1-a^2/rs^2)*(log(8*R0/a)-1)+log(a/rs))/(4*pi*R0);
kzc=(1+a^2/rc^2); kzs=(1-a^2/rc^2);
```

```
A=[-my0/(2*pi*rc^2) kzc; my0/(2*pi*rs^2) kzs];
B=[cos_ny-kpc*pla_ny; ver_ny-kps*pla_ny];


C=A\B; xI=C(1,:)'; x=C(1,:)./pla_ny; xone=ones(size(x));
x=min(x,xone*0.02); x=max(x,-xone*0.02); Bz=C(2,:)';
```

C.2.6 conformdata2.m

Conforms the measured data from vertical field sensor, cosine coil and Rogowski coil to vectors having the same starting time and length.

```
function [t,dtmin,pla_ny,cos_ny,ver_ny]=conformdata2(nbr);

pla_str=strcat('pla_',int2str(nbr),'.dat');
cos_str=strcat('cos_',int2str(nbr),'.dat');
ver_str=strcat('ver_',int2str(nbr),'.dat');
[pla_t,pla_d]=loaddata(pla_str);        % Plasma current data
[cos_t,cos_d]=loaddata(cos_str);        % Cosine coil data
[ver_t,ver_d]=loaddata(ver_str);        % Saddle coil data (vertical flux)

pla_s=size(pla_t,1); cos_s=size(cos_t,1); ver_s=size(ver_t,1);

tstartmin=min(cos_t(1),ver_t(1));
tstartmin=min(tstartmin,pla_t(1));
tstartmax=max(cos_t(1),ver_t(1));
tstartmax=max(tstartmax,pla_t(1));
tstopmin=min(cos_t(cos_s),ver_t(cos_s));
tstopmin=min(tstopmin,pla_t(pla_s));
pla_dt=(pla_t(pla_s)-pla_t(1))/pla_s;
cos_dt=(cos_t(cos_s)-cos_t(1))/cos_s;
ver_dt=(ver_t(ver_s)-ver_t(1))/ver_s;

dtmin=min(ver_dt,min(pla_dt,cos_dt));

t=tstartmax:dtmin:tstopmin;

pla_ny=interp1(pla_t,pla_d,t,'cubic')*1e3;  % current measured in kA
cos_ny=2*interp1(cos_t,cos_d,t,'cubic');  % calibration error => 2*
ver_ny=interp1(ver_t,ver_d,t,'cubic');

t=t'/1e3;       % time measured in ms

% Assume integer multiple of dtmin
pla_nt=pla_dt/dtmin; ver_nt=ver_dt/dtmin; cos_nt=cos_dt/dtmin;
```

C.2.7 loaddata.m

Loads measurement data from ascii file and stores it in vector `data`.

```
function [t,data]=loaddata(fname)

fid=fopen(fname);
tmp=fscanf(fid,'%g');
s=size(tmp,1);
```

```
t=tmp(1:s/2);   % Assume even size
data=tmp(s/2+1:s); fclose(fid);
```

C.2.8 feedforward.m

Extracts data from the theoretical feed forward transfer function and approximates it by adding a high frequency pole.

```
Ff=-G4/(G);             % power supply (1/W) neglected
[z p k]=zpkdata(Ff);

z1=sum(z{1})-sum(p{1});
fr=1e5;
Ff1=k*tf([1 -z1],[1 fr])*(fr);
```

C.2.9 phasemargin4.m

Calculates cross-over frequency ω_c and controller parameters using the equations in section 4.3.

```
%
% Calculates the maximum cross-over frequency
% for a PD controller with power supply
% time delay T, phasemargin fim and derivative
% cut-off factor N.
% Also the derivate part frequency opd and
% controller gain K are calculated
%

om=(atan(sqrt((N.^2-1)./(N-1)))
    -atan(sqrt((N.^2-1)./(N.^3-N.^2)))-fim)./T;
opd=om./sqrt((N.^2-1)./(N-1));
K=om.^2.*sqrt((N.^2+N+1)./(N+2));

[ans ans Kg]=zpkdata(G); Kp=K/Kg;

PD=tf([1 opd],[1 N*opd])*Kp/H;
```

References

[1] G.R. Dyer G.H. Neilson and P.H. Edmonds. A model for coupled plasma current and position feedback control in the ISX-B tokamak. *Nuclear Fusion*, 1984.

[2] T. Glad and L. Ljung. *Reglerteknik. Grundläggande teori*. Studentlitteratur, second edition, 1989.

[3] J.Hugill and A. Gibson. Servo-control of plasma position in CLEO-tokamak. *Nuclear Fusion*, 1974.

[4] J. Brynolf P. Brunsell and G. Hellblom. A method for external measurment of toroidal equilibrium parameters. *Laboratory Report, TRITA-ALF 1992:01*, 1992.

[5] H. Tsui P. G. Noonan and A. A. Newton. Toroidal equilibrium in the reversed field pinch corrected by a vertical field. *Plasma Physics and Controlled Fusion*, 1985.

[6] K. Åström and T. Hägglund. *PID Controllers: Theory, Design and Tuning*. Instrument Society of America, second edition, 1995.